Antiferromagnetic writing in $BiFeO_3$ investigated by second harmonic generation imaging

J.-Y. Chauleau[1*], E. Haltz[1], S. Fusil[2], C. Carretero[2], M. Viret[1]

[1] Service de Physique de l'Etat Condensé, C.E.A. Saclay, France
[2] Unité Mixte de Physique CNRS/Thales, Palaiseau, France

**Also at Synchrotron SOLEIL*

Spintronic systems

Conventional spintronics: ferromagnetic metals

But: electronic currents add dissipation
→ use pure spin currents: FM Insulators

Antiferromagnetic spintronics:
No magnetization → insensitivity to external fields
No stray fields → increased information density
Dynamical properties → Faster communication

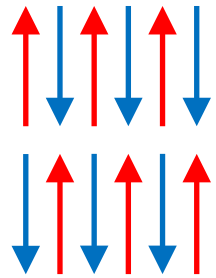

No dipolar field

→ Antiferromagnetic Insulators

Very common in nature
Many different magnetic structures/symmetry
Multifunctional materials
Superior dynamical properties (THz)

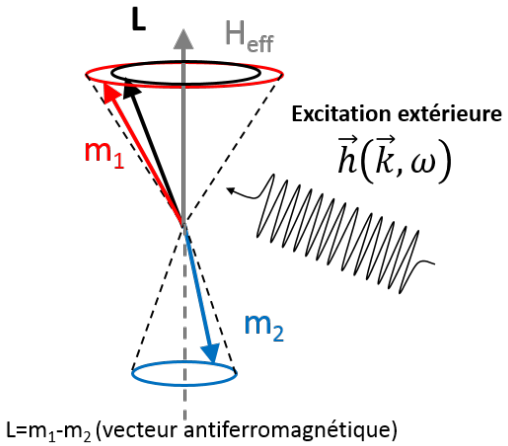

Prototypical antiferromagnet: NiO

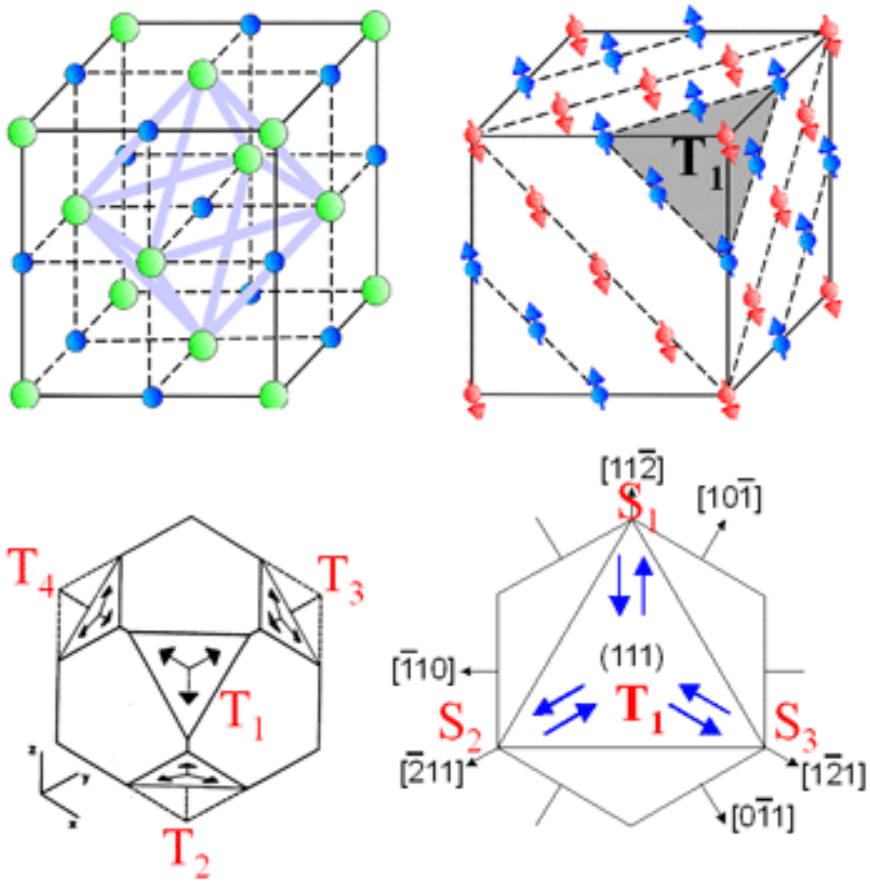

AF order in NiO:

4 T domains x 3 S domains = 12 possible AF domains
+ all of them present in thin films…

→ Multiferroics allow to reduce the number of variants

Multiferroics

Multiferroic materials:

Intrinsic coupling of several ferroic phases

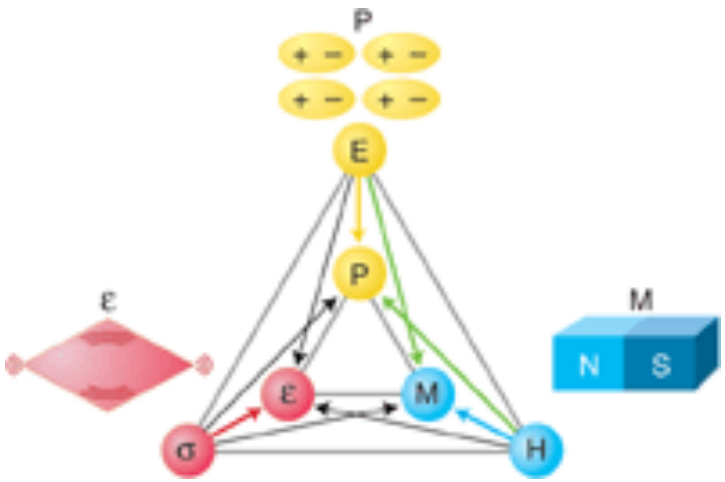

Spalding & Fiebig, Science, **309** *391* (2005)

Prototypical material: Bismuth Ferrite ($BiFeO_3$)

- *Ferroelectric*
- *Antiferromagnetic*

} At room temperature

Large ***Magneto-electric*** coupling

Route to electrical control of antiferromagnetism

$BiFeO_3$: ferroelectric, ferroelelastic and magnetic at 300K

Ferroelectric properties (T_C ~ 1090 K)

- Cubic perovskite structure → pseudo-cubic : rhombohedral distortion
- P_S due to Bi^{3+} and Fe^{3+} displacements along [111]

Ferroelectricity due to ordering of lone pairs:

2 outer 6s electrons of Bi not involved in chemical bonds

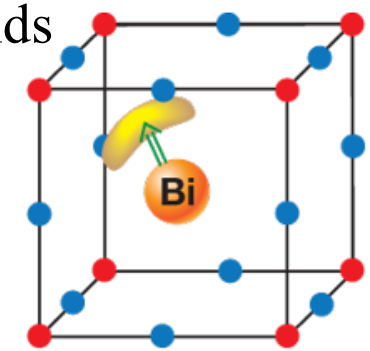

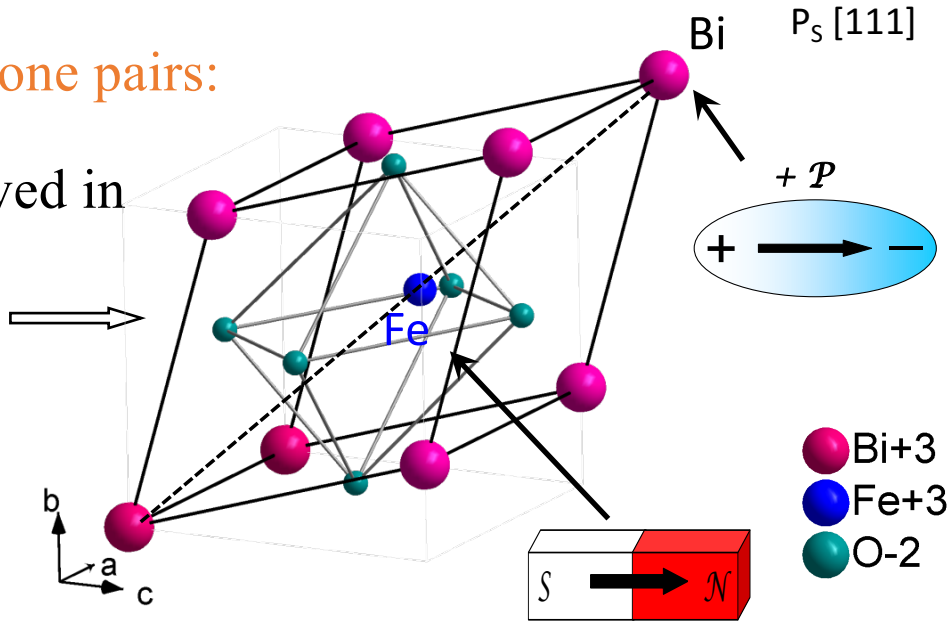

Large atomic displacements → large P_S

Kubel et al., Acta Cryst. B, 46 , 698 (1990)

Magnetic properties: G type AF + magnetoelectric coupling

Magneto-electric coupling in solids

In a solid with non-collinear magnetism (generalised Dzyaloshinski-Moriya interactions):

Typically oxydes with distorted crystallographic cells :

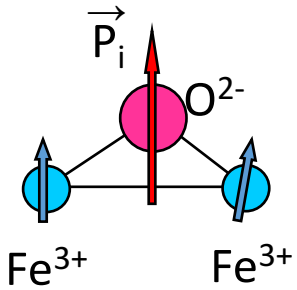

$$E_{DM} = \vec{D}_{ij} \cdot (\vec{S}_i \times \vec{S}_j)$$

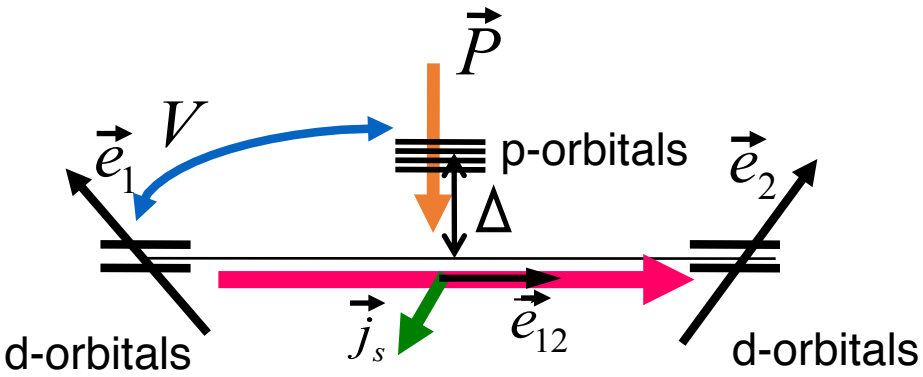

$$\vec{P} \propto \vec{e}_{12} \times \vec{j}_s$$

j_s = spin current

- P_S due to the magnetic structure

Katsura-Balatsky-Nagaosa PRL07

Leads to an AF cycloidal ordering :

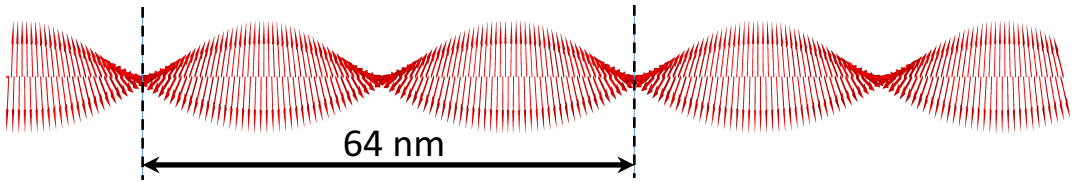

In strained thin films, the cycloid can be made unstable and an AF G-type with slight canting can be recovered

Second Harmonic Generation imaging

Second harmonic generation induced by :

- Spatial centro-symmetry breaking (ferroelectricity)
- Time-inversion symmetry breaking ((anti)-ferromagnetism)

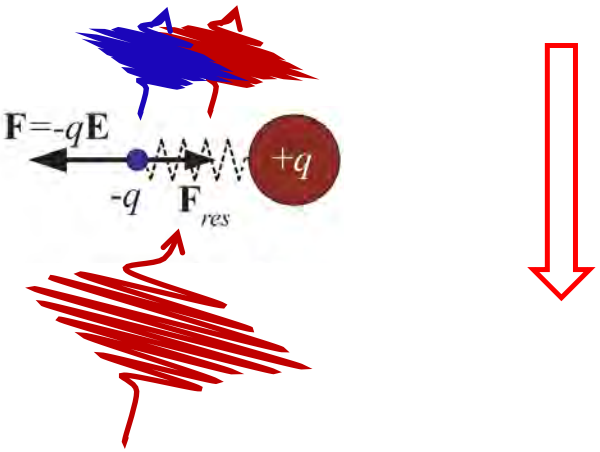

SHG Observation of coupled magnetic and electric domains in $YMnO_3$:

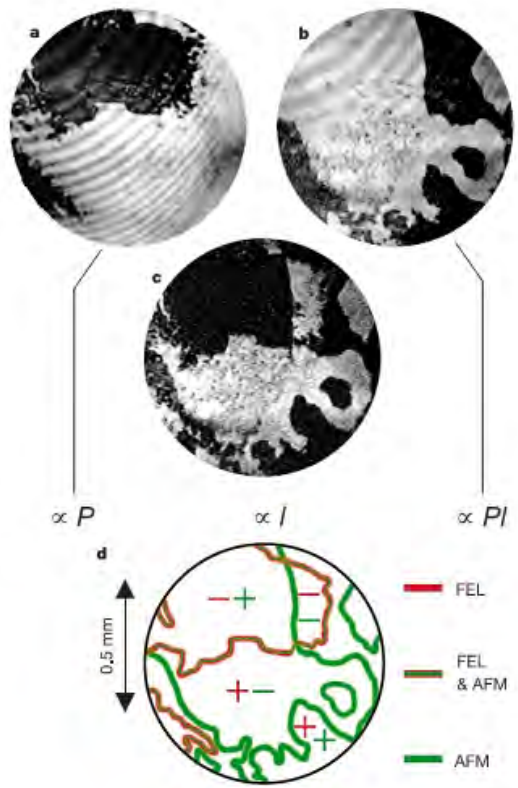

Elegant and powerful experimental approach to probe complex multiferroic textures and in particular antiferromagnetic order

Fiebig, Pavlov & Pisarev J. Opt. Soc. Am. B **22** 96 (2005)

Amplification of AF contrast for multiferroics due to P.L terms !

Fiebig, Lottermoser, Frölich, Goltsev & Pisarev Nature **419**, 818 (2002)

High resolution SHG wide field imaging

Experimental setup:

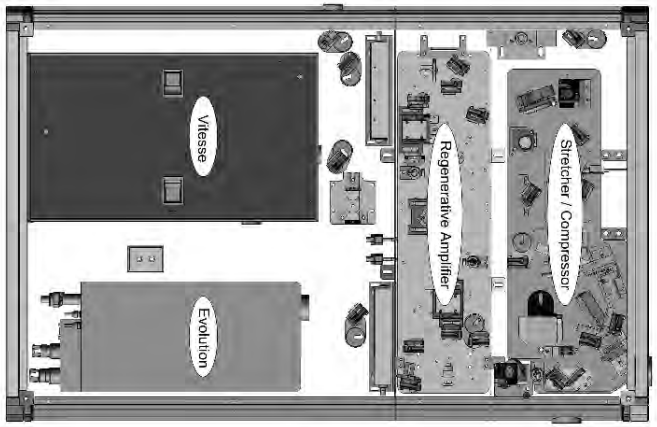

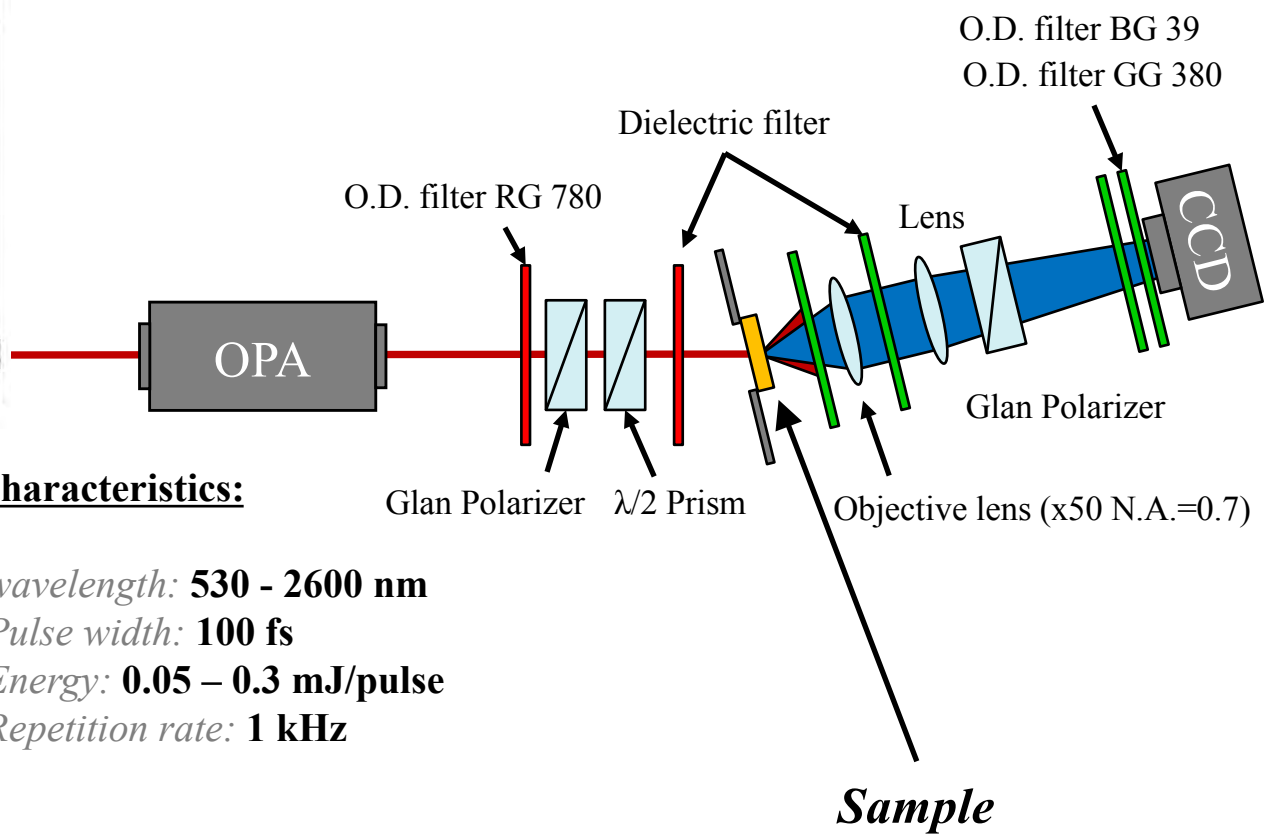

LIBRA characteristics:

- *wavelength:* **800 nm**
- *Pulse width:* **100 fs**
- *Energy:* **max. 4 mJ/pulse**
- *Repetition rate:* **1 kHz**

TOPAS characteristics:

- *wavelength:* **530 - 2600 nm**
- *Pulse width:* **100 fs**
- *Energy:* **0.05 – 0.3 mJ/pulse**
- *Repetition rate:* **1 kHz**

A signature of symmetry

Monoclinic second rank tensor (m) :

$$\begin{bmatrix} P_1^{2\omega} \\ P_2^{2\omega} \\ P_3^{2\omega} \end{bmatrix} = \begin{bmatrix} \chi_{111} & \chi_{122} & \chi_{133} & 0 & 0 & \chi_{112} \\ \chi_{211} & \chi_{222} & \chi_{233} & 0 & 0 & \chi_{212} \\ 0 & 0 & 0 & \chi_{323} & \chi_{313} & 0 \end{bmatrix} \cdot \begin{bmatrix} E_1^2 \\ E_2^2 \\ E_3^2 \\ 2E_2E_3 \\ 2E_1E_3 \\ 2E_1E_2 \end{bmatrix}$$

Rhombohedral second rank tensor (3m) :

$$\begin{bmatrix} P_1^{2\omega} \\ P_2^{2\omega} \\ P_3^{2\omega} \end{bmatrix} = \begin{bmatrix} \chi_{111} & 0 & 0 & 0 & \chi_{113} & 0 \\ 0 & 0 & 0 & \chi_{113} & 0 & -\chi_{111} \\ \chi_{113} & \chi_{113} & \chi_{333} & 0 & 0 & 0 \end{bmatrix} \cdot \begin{bmatrix} E_1^2 \\ E_2^2 \\ E_3^2 \\ 2E_2E_3 \\ 2E_1E_3 \\ 2E_1E_2 \end{bmatrix}$$

Below T_N, $BiFeO_3$ is 3m

According to Birss

$BiFeO_3$ thin films

Sample: STO/SRO/$BiFeO_3$ (001) (≈ 110 nm)

Possible electric/magnetic orders:

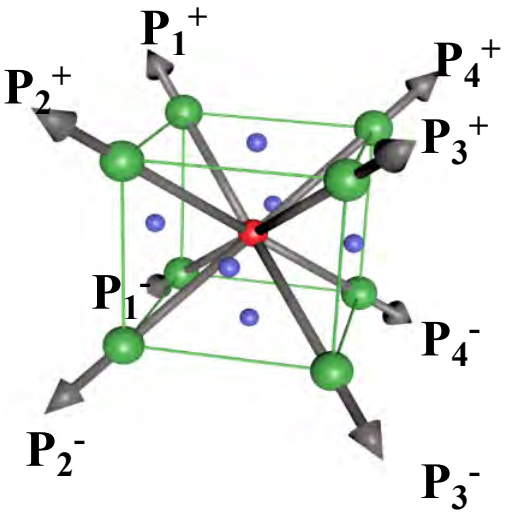

8 different polarization directions [111]

For each polarization, 3 possible spin orientations (*C. Ederer and N.A Spaldin, Phys. Rev. B* ***71****, 060401(R) (2005)*)

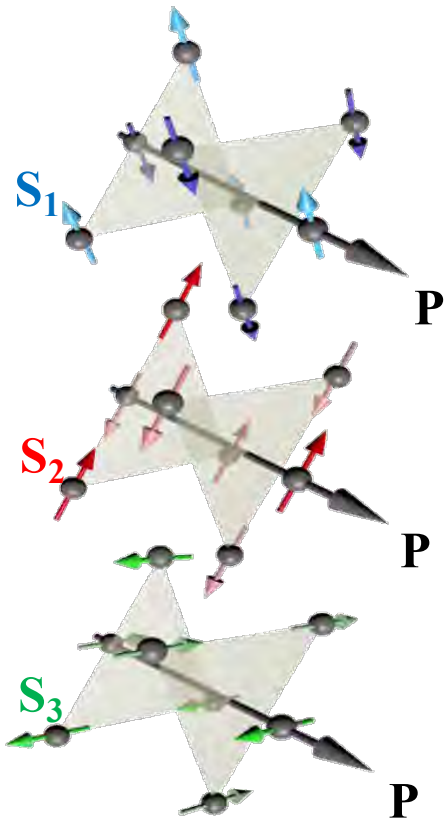

Ferroelectric configuration of the 001 $BiFeO_3$ epitaxial layer:

Out of plane P

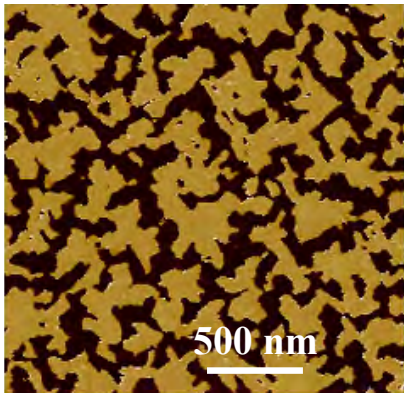

In-plane P

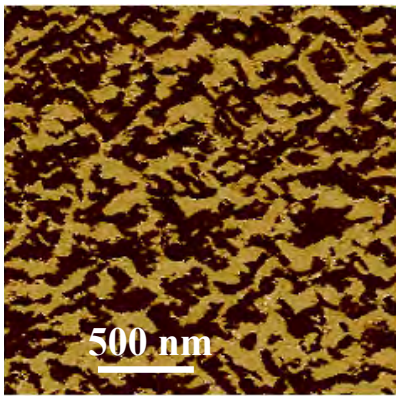

Writing FE domains

Definition of Ferroelectric monodomain patterns by Piezoresponse Force Microscopy (PFM) using the 'trailing field'

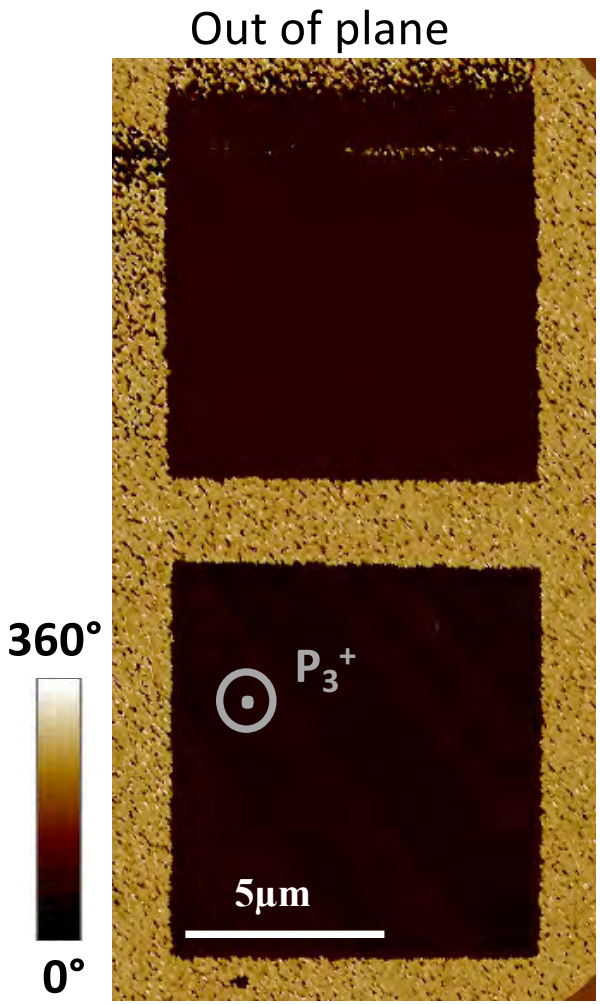

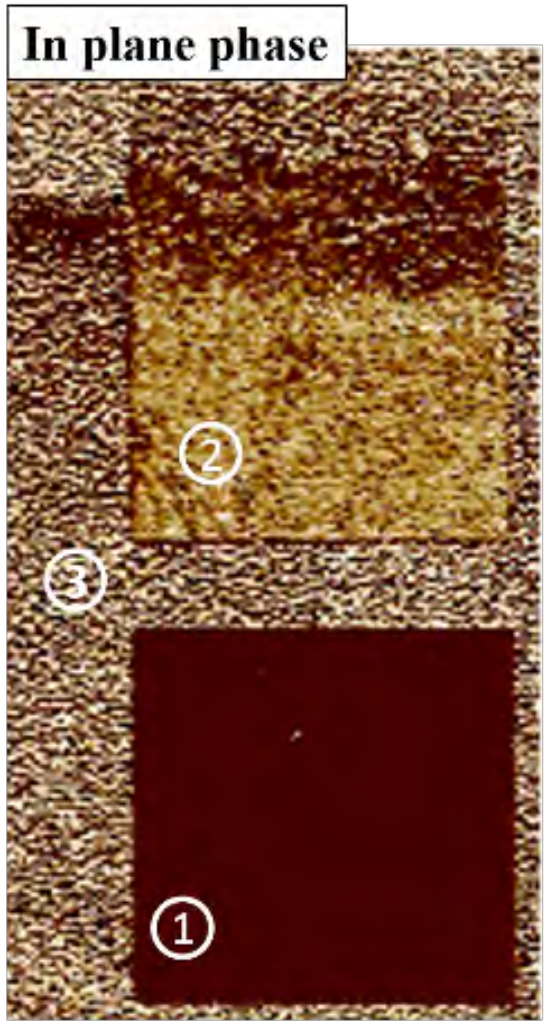

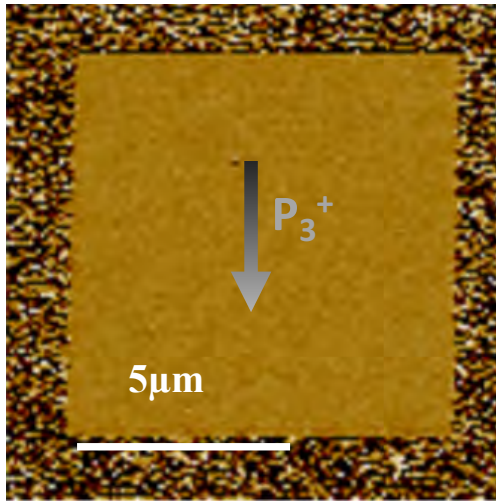

Second Harmonic Generation Spectroscopy

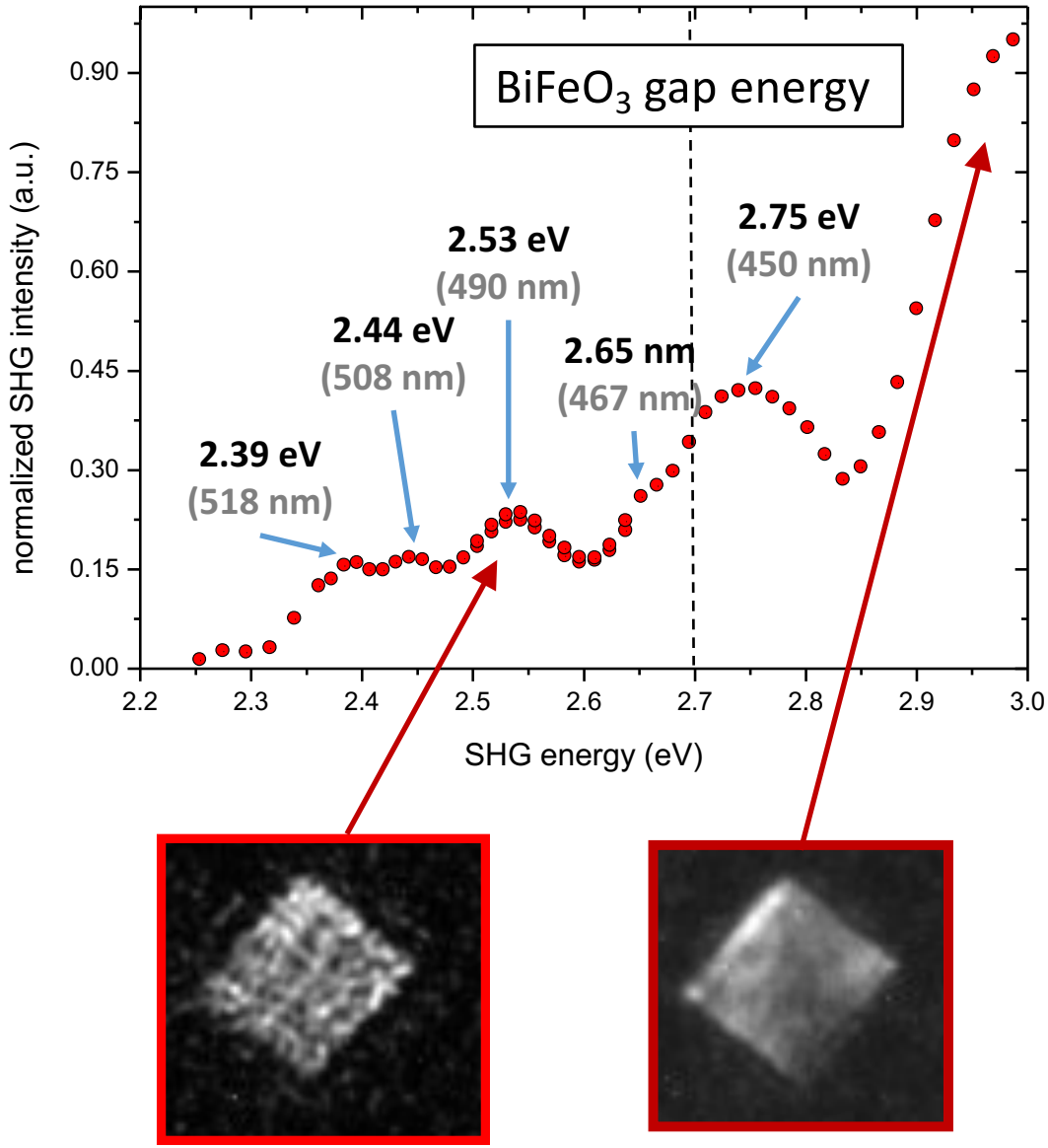

Magnon sidebands

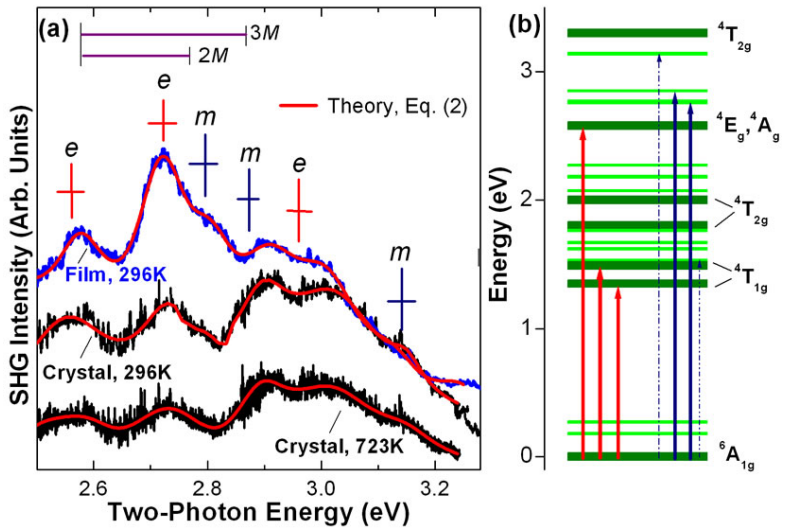

Ramirez & al. Phys. Rev. B **79**, 224106 (2009)

Second Harmonic Generation Imaging

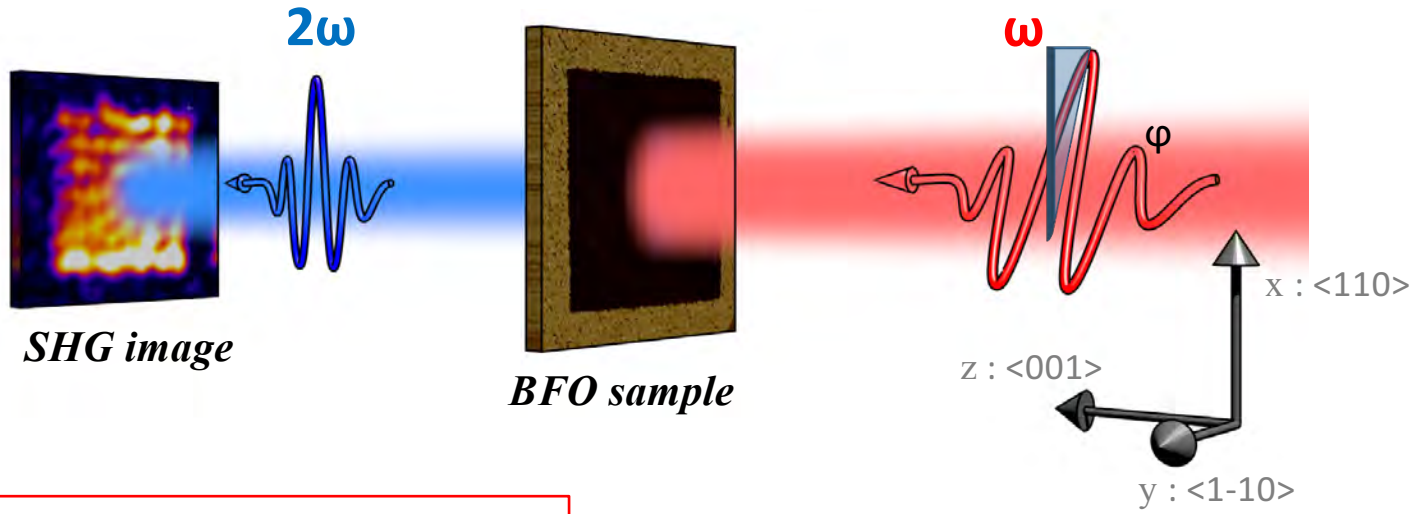

Nothing visible in linear optics !

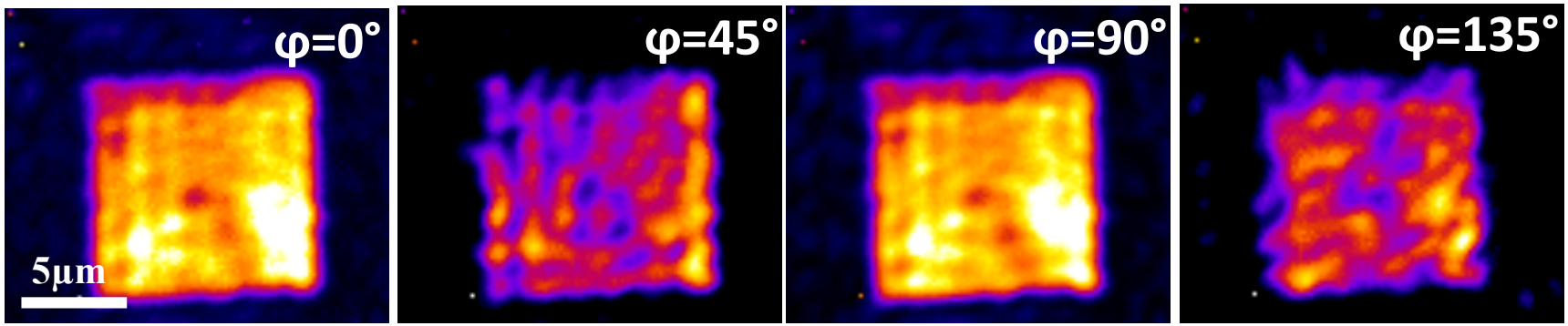

Set of typical SHG wide-field images for different linear incident polarisations φ analyzed along x. The color scale codes the SHG intensity.

Second Harmonic Generation Imaging

Full angular dependence on incident light polarization:

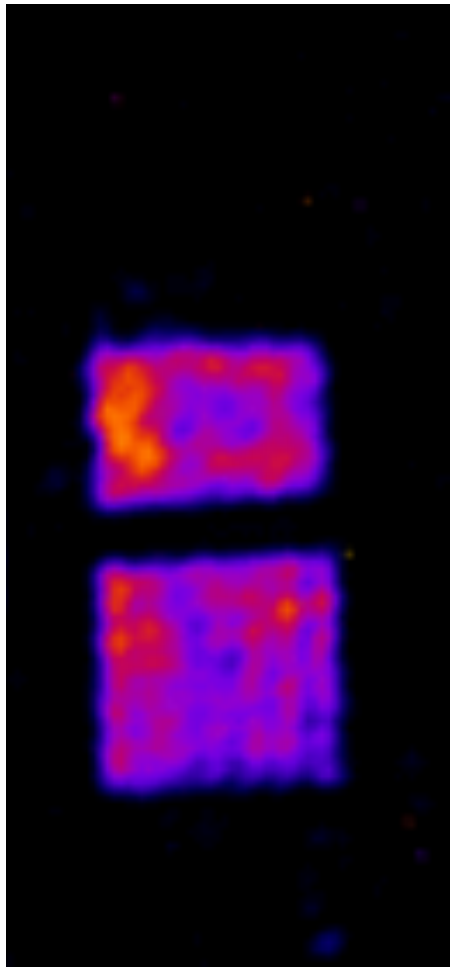

Second Harmonic Generation Imaging

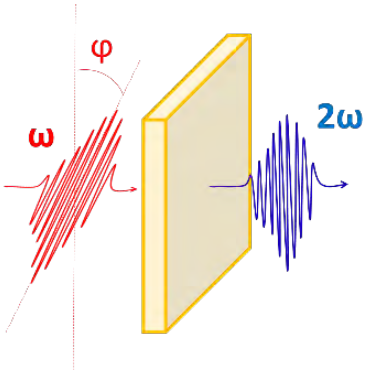

SHG angular dependence:

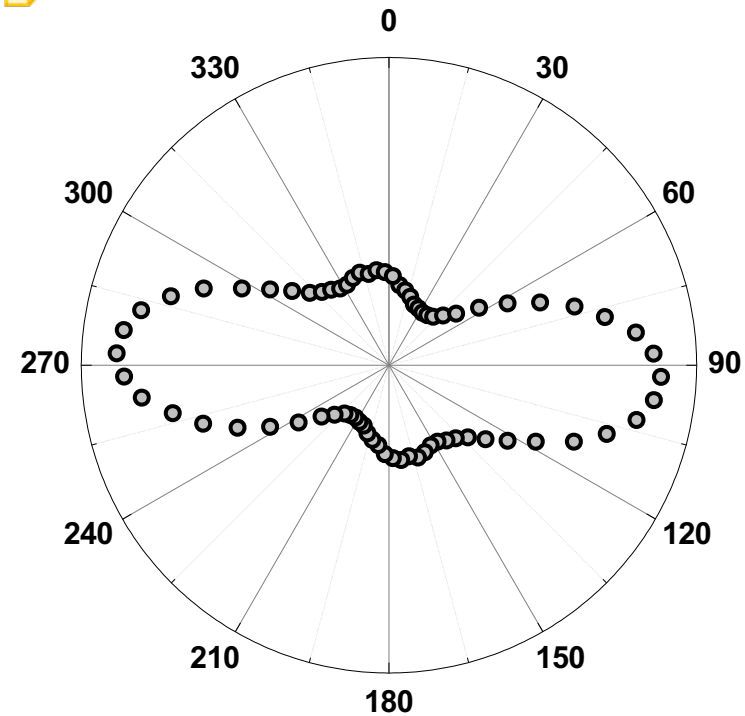

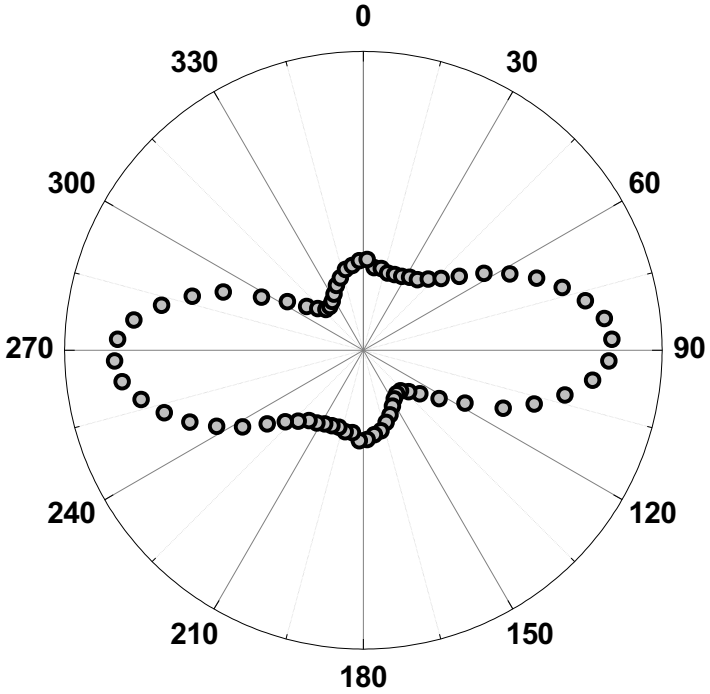

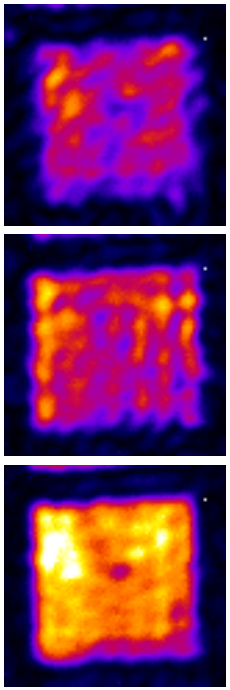

Two asymmetrical types of angular dependences are observed

Second Harmonic Generation Imaging

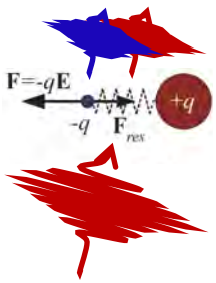

SHG angular dependence analysis:

Measured SHG intensity in the electron dipole approximation:

$$I_{SHG} \propto \left|\vec{P}\right|^2 \quad \text{with} \quad \vec{P} = \varepsilon_0\left(\chi^{(i)} + \chi^{(c)}\right) : \vec{E}(\omega) \otimes \vec{E}(\omega)$$

$\chi^{(i)}$ → *Time-invariant susceptibility:*
Crystallographic part, ferroelectricity

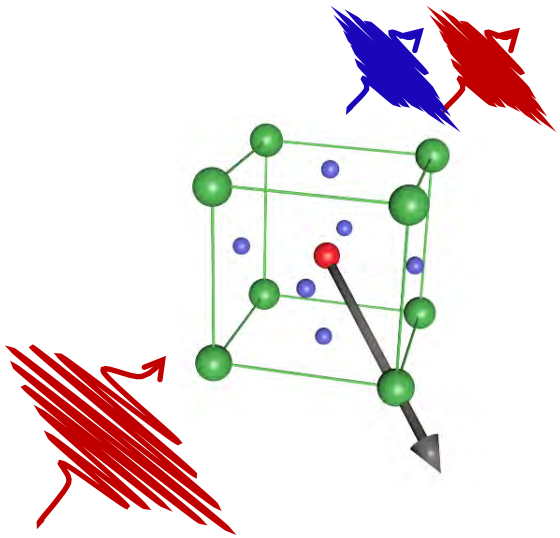

+

$\chi^{(c)}$ → *Time-**non**invariant susceptibility:*
Magnetic part

$$I_{2\omega} \sim \left(f^*(\chi_{ijk}) \cdot \sin^2\varphi + g^*(\chi_{ijk}) \cdot \cos^2\varphi + h^*(\chi_{ijk}) \cdot \sin\varphi\cos\varphi\right)^2$$

$f^*(\chi_{ijk})$, $g^*(\chi_{ijk})$ and $h^*(\chi_{ijk})$ complex functions

SHG analysis

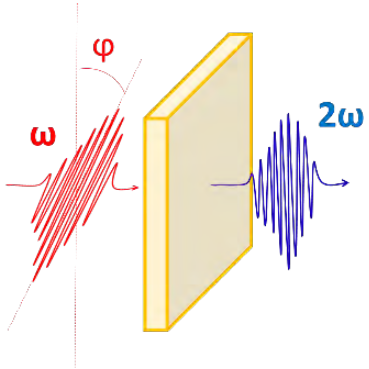

Three observed populations in SHG polar plots :

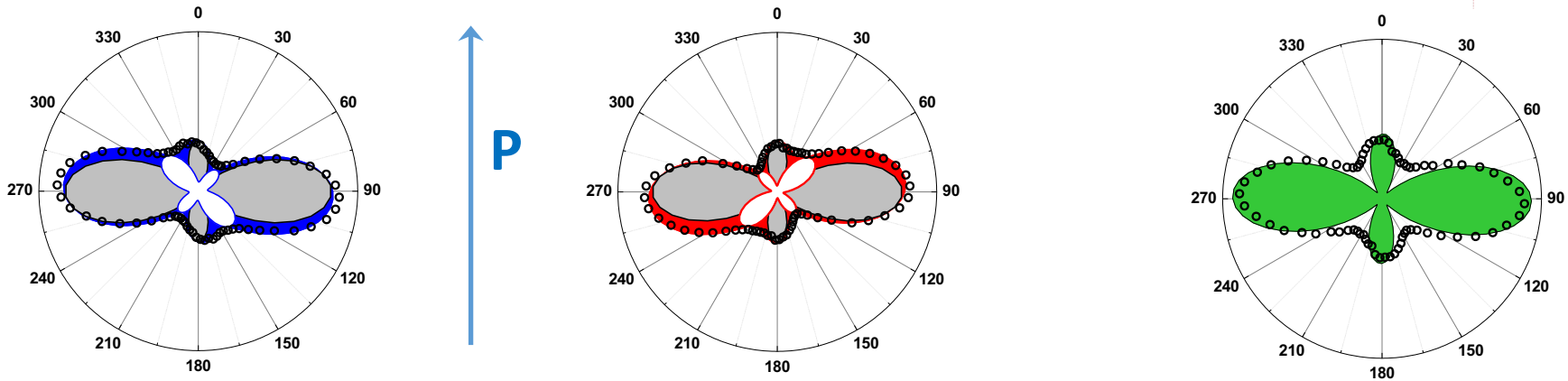

Open dots : experimental data

Red, blue and green filled areas: fits

In gray: time-invariant (ferroelectric) contribution
In white: time-noninvariant (antiferromagnetic) contributions:

$$P^{(c)}{}_{x\_type1} = a_1 \cos^2\varphi + b_1 \cos\varphi \sin\varphi + c_1$$

$$P^{(c)}{}_{x\_type2} = a_1 \cos^2\varphi - b_1 \cos\varphi \sin\varphi + c_1$$

$$P^{(c)}{}_{x\_type3} = a_3 \cos^2\varphi + c_3$$

Works well considering the projections of the 3 expected AF vectors

Second Harmonic Generation Imaging

Reconstructed AF image of the single FE domain:

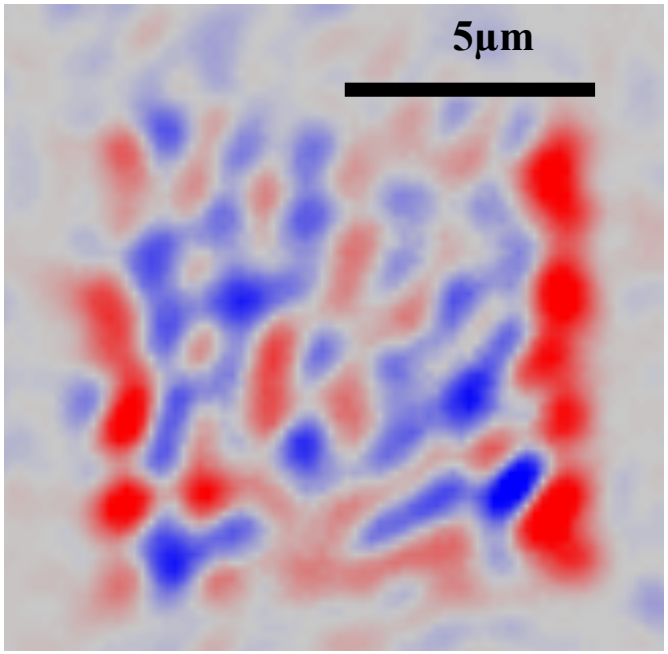

P [11]

The colour scale codes the asymmetry of the SHG polar plots

Blue: domains with L projecting along [10]

Red: domains with L projecting along [01]

White: domains projecting along [1-1] or DWs

AF domains ≈ 1μm in size

Second Harmonic Generation Imaging

The second FE multidomain (two variants) also shows AF domains in the micron range!

→ AF domains car be larger than FE ones !

→ granular random anisotropy models

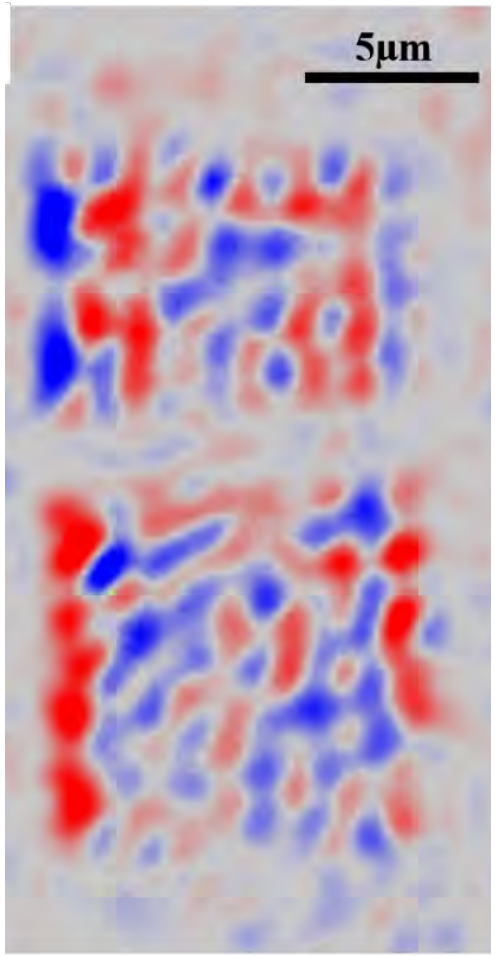

Imaging magneto-electric coupling

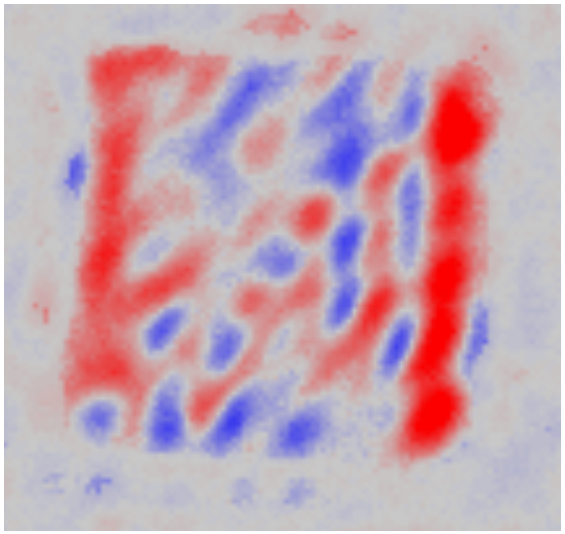

Initial AF image of a 8x8μm^2 single FE domain

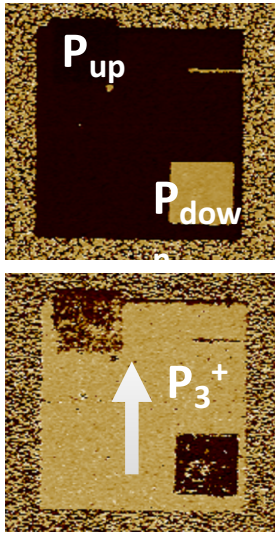

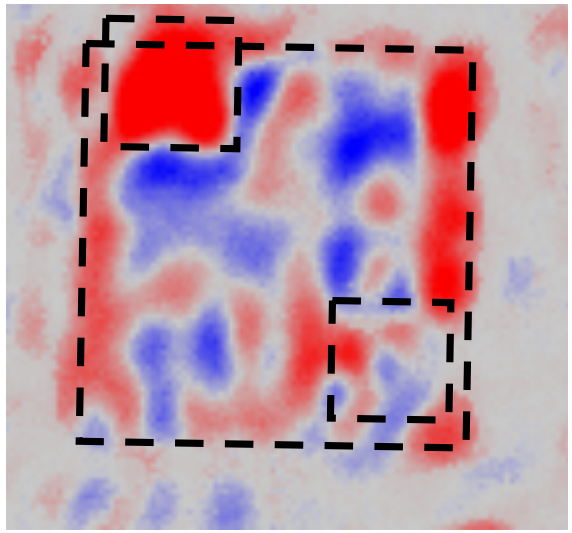

Final AF image showing changes in the AF structures

PFM images after re-writing two smaller 2.5x2.5 μm^2 squares.
Upper left : in plane switching
Lower right : out of plane switching

Manipulation of the AF order

A newly written FE pattern:

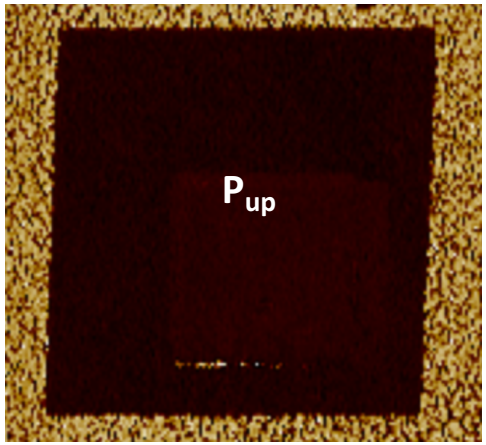

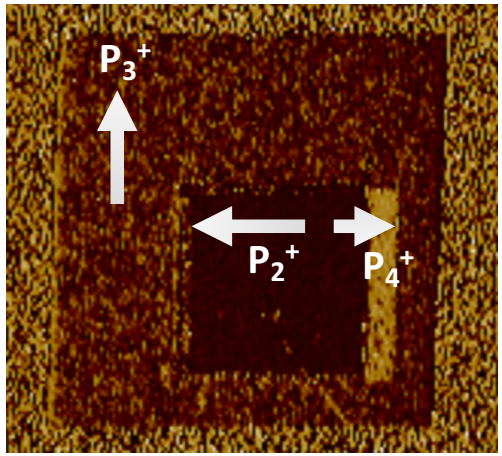

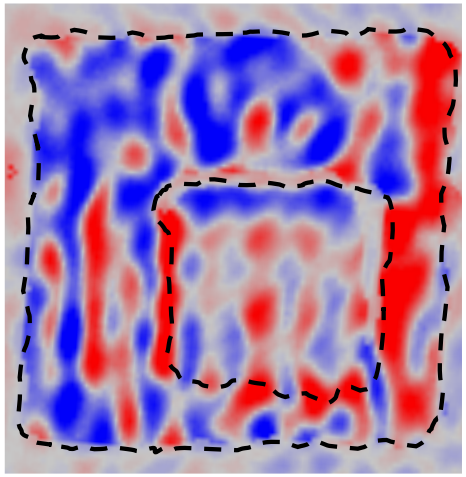

Out-of-plane and in-plane PFM images of an 8x8 µm² FE single domain square
Inner structures providing three polarization variants

Corresponding AF pattern

Manipulation of the AF order: heating

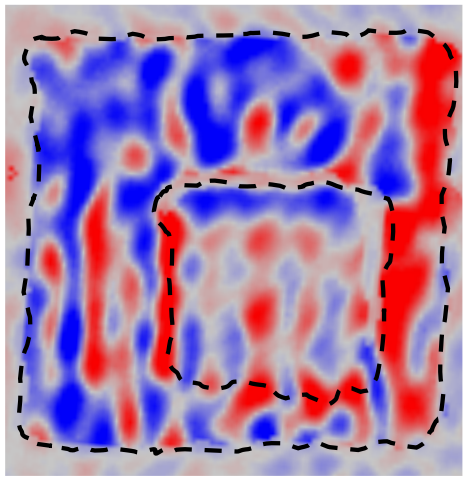

Initial AF image

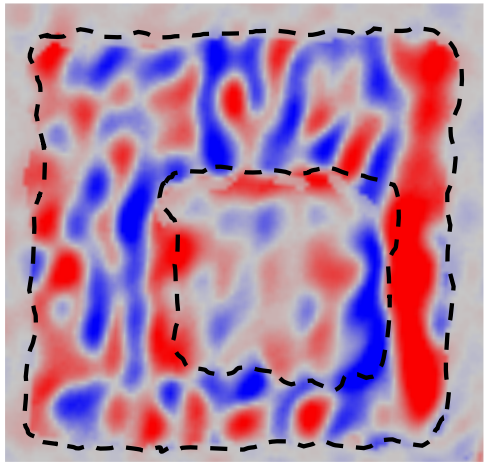

After heating to 570 K

→ **Heating below $T_{Néel}$** (640K) changes significantly the AF pattern

Manipulation of the AF order: Voltage

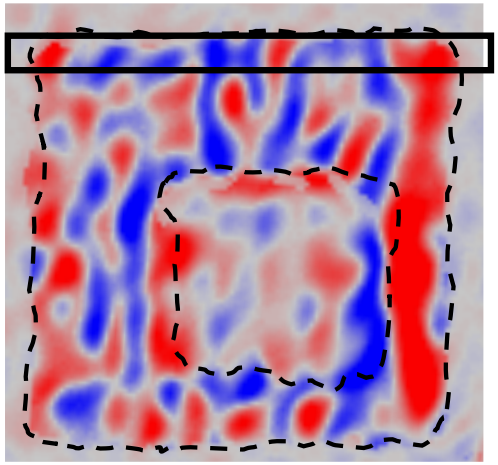

Initial AF image

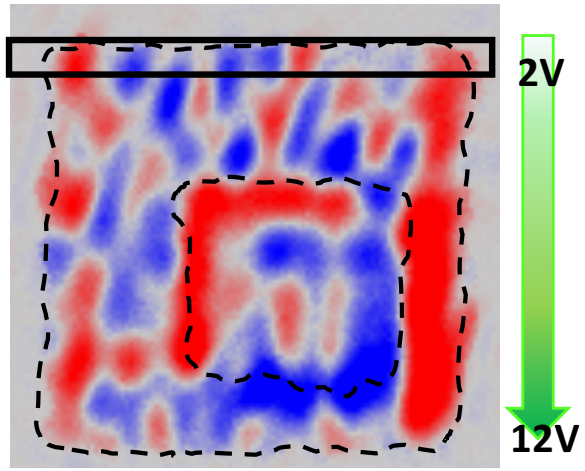

Final AF image after ramping
a DC voltage from 2V to 12V

→ **Voltages below the coercivity** (11V) can change significantly the AF pattern

Estimated in-plane trailing field at 3V ≈ 7 MV/m

Manipulation of the AF order: THz pulse

Optical rectification In BFO:

DC polarization induced due to the second-order nonlinearity:

$$P^{NL} = \chi^{(2)}(\cos\omega t)^2 = 1/2\chi^{(2)}(1+\cos 2\omega t) = P^{NL}(0)+P^{NL}(2\omega)$$

D.Talbayev et al., APL ***93****, 212906 (2008) :*

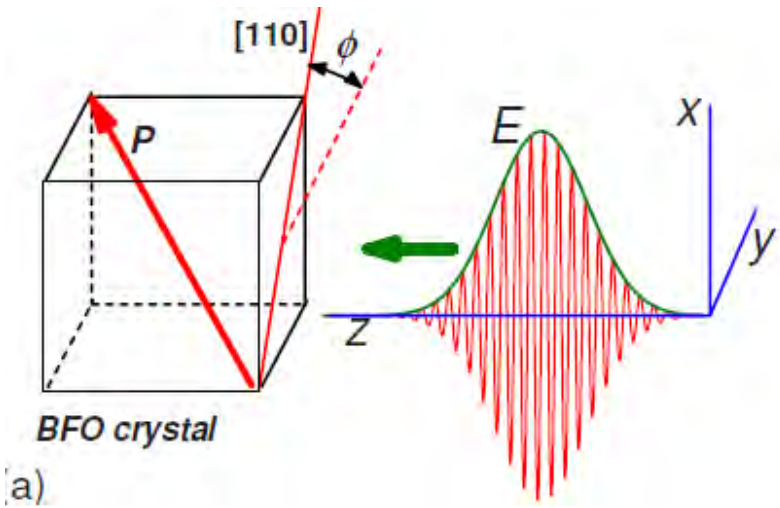

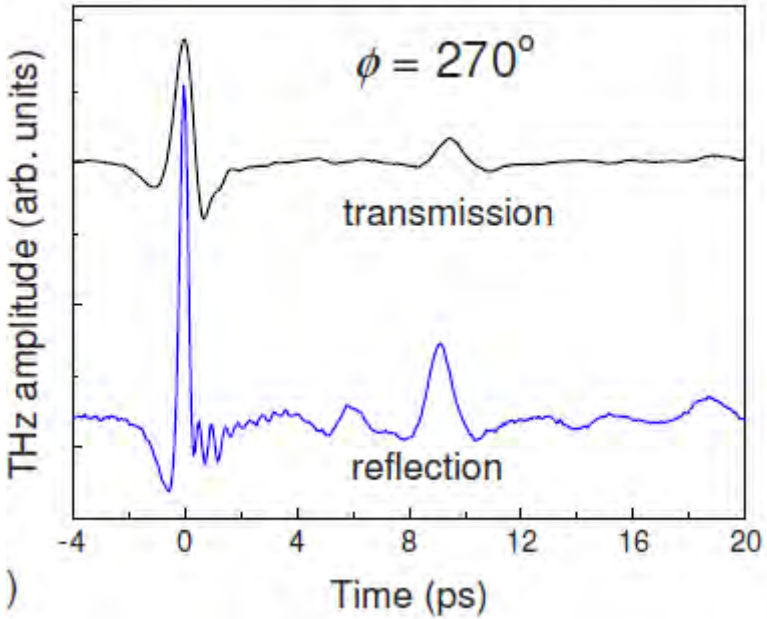

Manipulation of the AF order: THz pulse

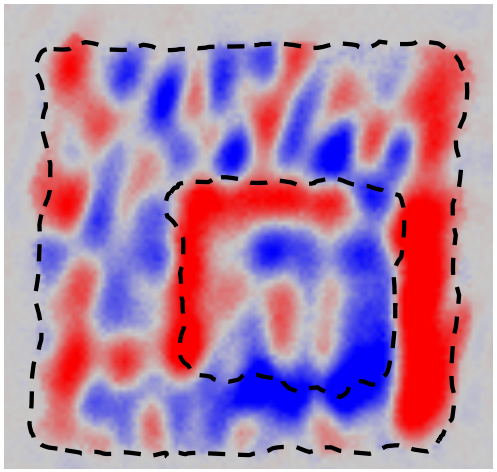

Initial AF image

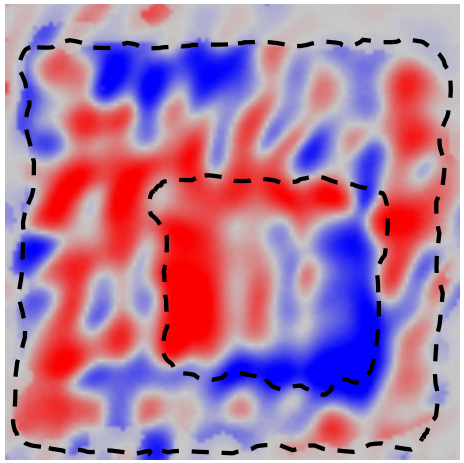

Final AF image after irradiation with fs laser pulses (925nm)

→ **THz laser pulses** significantly change the AF pattern

electric pulse estimated near 0.1MV/m

Conclusions

SHG is a powerful technique to image AF domains with submicron resolution.
It is especially well suited to insulators.

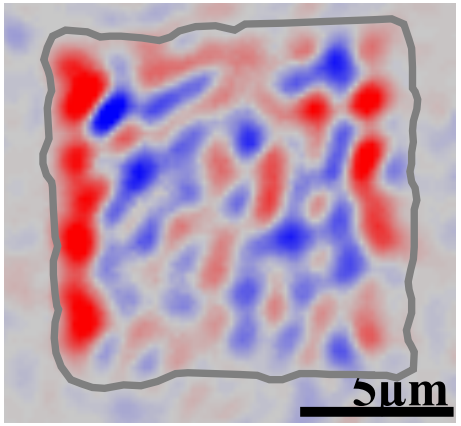

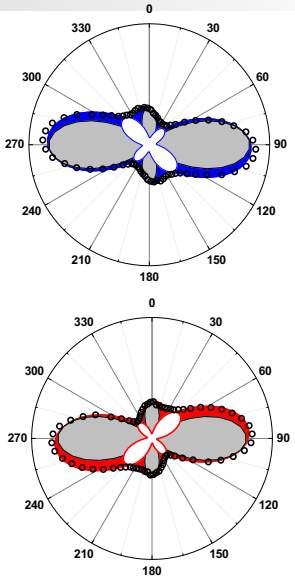

PFM image before PEEM:

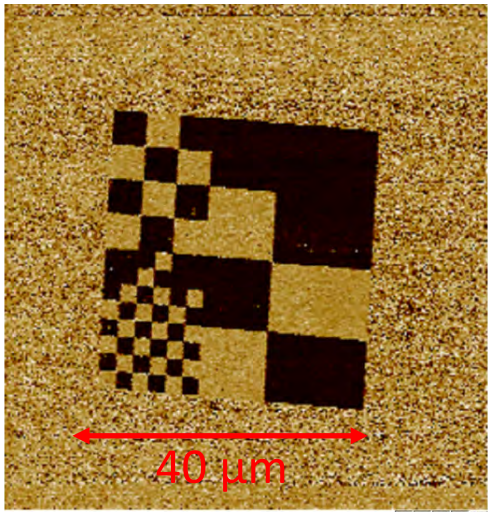

PFM image after PEEM:

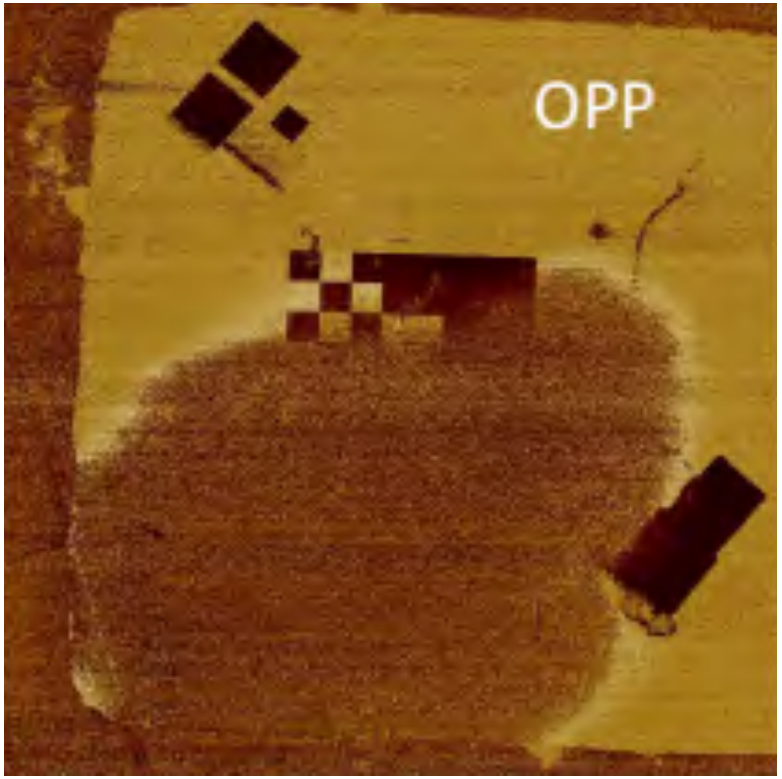

Conclusions

The 'natural' AF domain size in $BiFeO_3$ is in the micron range. The ME interaction is complex as AF domains can be larger or smaller than their FE counterparts

Two AF domains are degenerate in BFO films. They can be destabilised easily with temperature, small electric fields and THz pulses → all optical control?

Multiferroics offer the possibility to a two level coding of information: FE can be read with first harmonics, AF with second harmonics